J. Am. Soc. Mass Spectrom. (2017) 28:1324–1332
DOI: 10.1007/s13361-017-1600-8

FOCUS: BIO-ION CHEMISTRY: INTERACTIONS OF BIOLOGICAL IONS WITH IONS, MOLECULES, SURFACES, ELECTRONS, AND LIGHT : RESEARCH ARTICLE

Sulfur Pentafluoride is a Preferred Reagent Cation for Negative Electron Transfer Dissociation

Matthew J. P. Rush,[1,3] Nicholas M. Riley,[1,3] Michael S. Westphall,[3] John E. P. Syka,[4] Joshua J. Coon[1,2,3,5]

[1]Department of Chemistry, University of Wisconsin, Madison, WI 53706, USA
[2]Department of Biomolecular Chemistry, University of Wisconsin, Madison, WI 53706, USA
[3]Department of Genome Center, University of Wisconsin, Madison, WI 53706, USA
[4]Thermo Fisher Scientific, San Jose, CA 95134, USA
[5]Mordgridge Institute for Research, Madison, WI 53705, USA

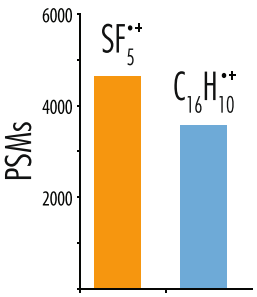

Abstract. Negative mode proteome analysis offers access to unique portions of the proteome and several acidic post-translational modifications; however, traditional collision-based fragmentation methods fail to reliably provide sequence information for peptide anions. Negative electron transfer dissociation (NETD), on the other hand, can sequence precursor anions in a high-throughput manner. Similar to other ion–ion methods, NETD is most efficient with peptides of higher charge state because of the increased electrostatic interaction between reacting molecules. Here we demonstrate that NETD performance for lower charge state precursors can be improved by altering the reagent cation. Specifically, the recombination energy of the NETD reaction—largely dictated by the ionization energy (IE) of the reagent cation—can affect the extent of fragmentation. We compare the NETD reagent cations of $C_{16}H_{10}^{\bullet+}$ (IE = 7.9 eV) and $SF_5^{\bullet+}$ (IE = 9.6 eV) on a set of standard peptides, concluding that $SF_5^{\bullet+}$ yields greater sequence ion generation. Subsequent proteome-scale nLC-MS/MS experiments comparing $C_{16}H_{10}^{\bullet+}$ and $SF_5^{\bullet+}$ further supported this outcome: analyses using $SF_5^{\bullet+}$ yielded 4637 peptide spectral matches (PSMs) and 2900 unique peptides, whereas $C_{16}H_{10}^{\bullet+}$ produced 3563 PSMs and 2231 peptides. The substantive gain in identification power with $SF_5^{\bullet+}$ was largely driven by improved identification of doubly deprotonated precursors, indicating that increased NETD recombination energy can increase product ion yield for low charge density precursors. This work demonstrates that $SF_5^{\bullet+}$ is a viable, if not favorable, reagent cation for NETD, and provides improved fragmentation over the commonly used fluoranthene reagent.

Keywords: Negative electron transfer dissociation, Mass spectrometry, Proteomics, Negative mode, Peptide anions, Electron transfer dissociation, Ion/ion reactions

Received: 22 November 2016/Revised: 6 January 2017/Accepted: 9 January 2017/Published Online: 27 March 2017

Introduction

Modern proteome characterization relies on liquid chromatography coupled with tandem mass spectrometry (nLC-MS/MS) to detect and quantify proteins from complex biological samples [1–5]. Despite continual advances in proteomic depth achieved in such experiments, these technologies do not detect all the proteins present in a sample and, in fact, typically only monitor a portion of those proteins that are detected. More specifically, one or two peptides resulting from the enzymatic digestion of a protein can map uniquely to the parent protein and allow for its unambiguous detection and quantification. New approaches that can offer increased diversity of peptides measured are therefore of considerable significance as they can reveal new proteins and offer access to portions of proteins that were previously not detectable. One factor that may limit the scope of the present technology is the

Electronic supplementary material The online version of this article (doi:10.1007/s13361-017-1600-8) contains supplementary material, which is available to authorized users.

Correspondence to: Joshua J. Coon; *e-mail:* jcoon@chem.wisc.edu

unilateral use of positive electrospray ionization. Many proteins, and portions of most proteins, are acidic and thus are more easily ionized in the negative mode [6–8]. Negative electrospray ionization can generate multiply deprotonated peptide anions, but the commonly used collision-based dissociation methods are ineffective at producing sequence-informative fragmentation of negatively charged peptides [9, 10]. These limitations have driven the development of alternative dissociation methods for peptide anions that utilize electrons, photons, and metastable atoms [11–30].

Scott McLuckey, the recipient of the Award for Distinguished Contributions in Mass Spectrometry, whom we honor in this issue of JASMS, has been a pioneer in this field, especially in the development of gas-phase ion–ion chemistry [31, 32]. Indeed, this investigation stems from foundational work his group and others described. Most notably, in 1995 McLuckey and co-workers first introduced ion–ion reactions of positive reagent cations with anionic oligonucleotides, and have continued this innovating in this space [33–35]. Inspired by McLuckey's experiment, we developed ion–ion reaction chemistries to abstract electrons from multiply deprotonated peptide anions using singly charged reagent cations, termed negative electron transfer dissociation (NETD) [11]. NETD has emerged as one of the most promising peptide anion dissociation methods and has been successfully utilized in nLC-MS/MS experiments to access the acidic proteome [11, 12, 16, 17, 30].

One challenge of using NETD in large scale proteomic experiments is its limited product ion yield for low charge density precursors. In NETD experiments, peptide anions are oxidized by positively charged reagent cations to initiate dissociation and production of $a^{\bullet}$- and *x-type* product ions. Sometimes electron transfer from the anion to the cation occurs without concomitant dissociation (i.e., non-dissociative negative electron transfer, or NETnoD) [36–39]. NETnoD frequently occurs and is one of the primary causes for reduced product ion yields in NETD, especially in the case of low charge density precursors [39]. In these cases, once electron transfer has occurred, peptide backbone cleavage may be achieved; however, the resultant product ions can be held together by noncovalent bonding and detected as a charge-reduced product. To maximize the production of NETD product ions, a reduction of NETnoD species can be accomplished by supplying the charge-reduced product with more energy, either concurrent with, or post- electron transfer. The additional energy can disrupt the noncovalent interactions holding these ions together, yielding sequence informative products [40, 41]. One such approach, termed activated-ion NETD (AI-NETD), has been implemented by concurrently irradiating the ions with infrared photons as they are interacting; however, this approach requires the addition of an IR laser to the system [16, 30].

An alternate approach to increase the energy of the system during electron transfer events is to alter the reaction exothermicity, which is determined by the difference between the ionization energy of the reagent cation and the electron affinity of the peptide anion. For example, the ionization energy of fluoranthene, $C_{16}H_{10}^{\bullet+}$, is 7.9 eV and the electron affinity of the carboxylate ion of a peptide is 3.4 eV, yielding a reaction enthalpy of 4.5 eV, known as the recombination energy. This energy surplus is redistributed into the peptide anion and drives fragmentation. Use of NETD reagent cations with higher ionization energies result in increased recombination energies and, potentially, an increase in NETD fragmentation efficiency [42]. The recombination energy of the reagent cation and its effect on NETD has been previously explored by Polfer and co-workers for use in determining phosphorylation sites on standard peptides [43], as well as by McLuckey et al. to investigate transition metal complexes and their interaction with peptide anions [44]. Polfer and colleagues compared two NETD reagents (fluoranthene and xenon) and determined that the increase in ionization energy of xenon led to considerable phosphate and side-chain neutral loss and, therefore, fluoranthene, having a lower ionization energy than xenon, should be used for sequencing phosphopeptides. Alternatively, McLuckey and co-workers showed that transition metal complexes yield electron transfer as well as metal insertion reactions, allowing further control of the cation–anion interaction. To date, only xenon, fluoranthene, and phenanthroline complexes of Fe, Cu, and Co have been investigated as NETD reagent cations for peptide analysis, and fluoranthene remains by far the most commonly used NETD reagent.

The primary motivation of this work is to investigate the hypothesis that increasing the ionization energy of the NETD reagent cation will increase the NETnoD conversion to product ions, thereby yielding greater peptide identification rates and protein sequence coverage in large-scale shotgun proteome analyses. To test this hypothesis, we used a set of synthetic peptides to compare the NETD fragmentation efficiency of sulfur pentafluoride cations ($SF_5^{\bullet+}$, IE = 9.6 eV) and fluoranthene cations ($C_{16}H_{10}^{\bullet+}$, IE = 7.9 eV) over a range of available precursor charge states ($z = -2$ to -6). Concluding that $SF_5^{\bullet+}$ cations provided increased sequence ion production for low charge state precursors, we then performed nanoflow liquid chromatography-tandem mass spectrometry (nLC-MS/MS) experiments employing high pH separations and optimized NETD reaction kinetics to compare $C_{16}H_{10}^{\bullet+}$ with $SF_5^{\bullet+}$ NETD reagent ions for analysis of a complex mixture of yeast peptides. From these data, we revealed that up to 40% more peptide spectral matches (PSMs) could be made when using reagent ions from sulfur pentafluoride compared with fluoranthene. The overall peptide spectral match and unique peptide identification numbers improved 30% when using $SF_5^{\bullet+}$ as the NETD reagent instead of fluoranthene. From the data, we conclude that the use of $SF_5^{\bullet+}$ offers a direct route to boosting the performance of NETD dissociation.

Experimental

NETD on Standard Peptides

Synthetic peptides that have the sequences SVFAVNWISYLASK, EEAQALEDLTGFK, and ELVNDDEDIDWVQTEK were obtained from New England Peptides (Gardner, MA, USA) and were individually

suspended in 3:1 methanol/water with 5 mM piperidine to a concentration of 10 ppm. The peptides were infused into a LTQ Velos mass spectrometer (Thermo Fisher Scientific, San Jose, CA, USA) modified to perform NETD. For each peptide precursor, a 0 nce CAD MS/MS scan was performed, followed by a series of NETD MS/MS scans with increasing reaction time, encompassing the 2τ time point (see Supplementary Figure 1 for further experimental design diagram). This series was repeated at least 15 times. Once complete, the next precursor charge state was reacted until all accessible charge states were reacted. The precursor AGC target was set to 10,000 and the reagent AGC target was set to 1,000,000 for all MS/MS acquisitions. The q-value for the NETD reaction was kept at 0.4 for all experiments. This procedure was repeated using both $SF_5^{\bullet+}$ and $C_{16}H_{10}^{\bullet+}$ reagent cations. The solid phase NETD reagent fluoranthene was introduced to the system using the standard glass vials contained in the ETD module's reagent vial heater. The gaseous sulfur hexafluoride reagent was introduced to the system by connecting the high purity SF_6 gas cylinder (Concorde Specialty Gases, Eatontown, NJ, USA) to a precision regulator (Porter Instruments, Hatfield, PA, USA) with 6 feet of 1/8 inch outer diameter and 0.065 inch inner diameter copper tubing. Then a 100 μm inner diameter capillary tube was attached to the out port of the precision regulator and fed directly into the vacuum manifold of the ETD module and the pressure reading of the precision regulator was adjusted to generate appropriate reagent cation signal (~2 psi). Reagent cations were generated via the EI/CI source in the presence of nitrogen gas, and reagent signal was optimized by varying lens voltages using an automated calibration routine. The filament emission current was set to 70 μA for both reagents. The nitrogen gas pressure was also optimized for maximum signal for each reagent cation. For fluoranthene, the reagent vial temperature was set to 108 °C. For both reagents, the ion source, transfer line, and restrictor temperature were held at 160 °C. The fluoranthene reagent produced ion radicals $C_{16}H_{10}^{\bullet+}$, whereas the predominant cation for sulfur hexafluoride was the fluorine-loss species $SF_5^{\bullet+}$, shown in Supplementary Figure 2.

Yeast Sample Preparation

Tryptic yeast (*Saccharomyces cerevisiae*) peptides were prepared as previously described [16]. Briefly, cultured yeast cells were lysed by glass bead milling (Retsch GmnH, Germany), and proteins were reduced and alkylated using 5 mM dithiothreitol and 15 mM iodoacetamide, respectively. Trypsin digestion was performed during an overnight incubation at room temperature with a 1:50 (w/w) enzyme to protein ratio. A second trypsin addition was done the following morning at 1:100 (w/w) enzyme to protein ratio for 1 h, followed by desalting over a C18 SepPak (Waters Corporation, Milford, MA, USA).

High pH nLC-MS/MS

An ETD-enabled hybrid dual cell-quadrupole ion trap-Orbitrap mass spectrometer (Orbitrap Elite, Thermo Fisher Scientific) coupled to a nanoACQUITY UltraPerformance liquid chromatograph (Waters) was used for the nLC-MS/MS analyses. The mass spectrometer was modified to perform NETD as described previously [41, 45–47]. Briefly, the higher energy collisional dissociation cell (HCD) was replaced with a multipurpose dissociation cell (MDC) that can conduct ion–ion reactions, allowing for NETD to be performed within. Fluoranthene and sulfur hexafluoride reagents were introduced as is described above, with the exception of the SF_6 pressure being adjusted to 10 psi. The solvent compositions for liquid chromatography were mobile phase A (5 mM piperidine in water) and mobile phase B (5 mM piperidine in 85% ACN and 15% water). The reverse phase columns were prepared in-house using 75 μm i.d., 360 o.d. bare fused silica capillary tubing packed to a 30 cm length with 3.5 μm, 130 Å pore size, Ethylene Bridged Hybrid C18 particles (Waters). For each analysis, 1 μg of yeast digest was loaded onto the column equilibrated with 95% A at 400 nL/min. The gradient elution was performed at 400 nL/min increasing from 5% mobile phase B to 30% B over 70 min, followed by an increase to 70% B at 76 min and a wash at 70% B for 4 more min. Peptides were ionized in the negative mode using electrospray ionization with a spray voltage of –1.5 kV. The inlet capillary temperature was set to 300 °C. Survey MS scans were analyzed in the Orbitrap mass analyzer with a resolving power of 60,000 at 400 *m/z* and an AGC precursor ion target value of 1,000,000 over a mass range of 300–1250 *m/z*. Data-dependent MS/MS events were triggered off of the 10 most intense peaks in the survey scan. Each MS/MS scan used a precursor AGC target of 100,000 ions and was analyzed in the Orbitrap with a resolving power of 15,000 at 400 *m/z*. Precursors were isolated at ±0.9 Th and an exclusion window of ±10 ppm was created around the monoisotopic peak of the precursor for 45 s. All nLC-MS/MS experiments were performed in duplicate.

Data Analysis

Peptide standard infusion data were searched using an in-house C# script, which extracted ion current intensities directly from raw data files. These values were normalized relative to the ion current of the precursor from a 0 nce CAD scan collected previous to the NETD reacted spectra (see Supplementary Figure 1 for further experimental design diagram). The nLC-MS/MS raw data files were searched using the open mass spectrometry search algorithm (OMSSA), modified to allow for anionic peptide $a^{\bullet}$- and *x-type* fragment ions to be searched. Search parameters included carbamidomethylation of cysteine as a fixed modification and oxidation of methionine as a variable modification [17, 48]. A multi-isotope search was employed using three isotopes with a mass tolerance of ±125 ppm for the precursors and a monoisotopic mass tolerance of ±0.02 Da for product ions. Three missed cleavages were allowed for the trypsin digestion. The data processing was done through the COMPASS software suite designed for OMSSA searching. A UniProt database for *Saccharomyces cerevisiae* (downloaded September 29, 2014) was

concatenated with reversed sequences and used to determine peptide spectral matches (PSMs). Scored spectra were filtered using a false discovery rate of 1% at the unique peptide level. False discovery rates for spectra from each set of duplicate nLC-MS/MS experiments were calculated for the combined set of spectra as opposed to separate calculations for each nLC-MS/MS run. Additionally, prior to OMSSA searching, each spectrum was preprocessed to remove the unreacted precursor ion (±3 Da) and neutral loss ions of the oxidized precursor by removing ions within a window of 55 to 5 Da below the oxidized precursor ion. The nLC-MS/MS experiments were also searched using an in-house C# script to extract ion intensities for expected sequencing ions as well as ions resulting from neutral losses from both oxidized precursor ions and $a^{\bullet}$- and *x-type* product ions. Ion intensities from spectra in nLC-MS/MS experiments were normalized relative to the total ion current (TIC) of each individual MS/MS scan.

Results and Discussion

NETD of Standard Peptides with Alternative Reagent Cations

The primary metric in determining an effective reagent cation is the production of sequence informative fragment ions relative to all other product ions produced. In these experiments, reagent ions $C_{16}H_{10}^{\bullet+}$ and $SF_5^{\bullet+}$ were tested for their effectiveness as NETD reagent cations using an ETD-enabled dual-pressure linear ion trap mass spectrometer. These species were reacted with three standard peptides (sequences given in top left of Figure 1), each with a C-terminal lysine to mimic those yielded from protein digestion with trypsin, and all were synthesized without additional post-translational modifications. The peptides had lengths of 13, 14, and 16 amino acid residues, isoelectric points of 3.62, 4.00, and 8.31, and generated peptide anions having charge states ranging from $z = -2$ to -6.

To provide a straightforward comparison of their product ion generation efficiencies, the extent of reaction for the two reagent cations was carefully controlled. To do so, we standardized several conditions that dictate the number of electron transfer events that occur per reaction, isolating the chemistry of the reagent cations as the main variable of the experiment. The rate of ion–ion reactions and, thus, the number of electron transfer events, are governed by a number of parameters, including ion population, reaction q-value, reaction cell architecture, and reaction time. Previous work has shown that to maximize peptide identifications, the ideal electron transfer extent occurs when the precursor ion population has been reduced by 86% [49]. Such reaction conditions minimize the amount of secondary electron transfer while still offering sufficient sequence informative fragment ion production. Using this as a model, we created a method, illustrated in Supplementary Figure 1, where a series of increasing reaction times were employed surrounding the optimal reaction extent (13.5% unreacted precursor remaining), keeping all other reaction parameters constant. Figure 1 summarizes the production of

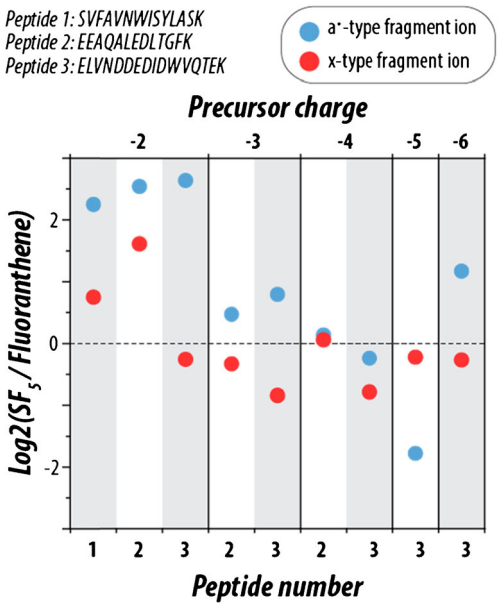

Figure 1. Comparison of product ion signal from NETD reactions using reagents $C_{16}H_{10}^{\bullet+}$ and $SF_5^{\bullet+}$ for all precursor charge states of three synthetic peptides (sequences shown top left). The intensities of both $a^{\bullet}$- and *x-type* fragment ions were normalized to the total ion current of the unreacted precursor from a preceding scan as explained in the text. Following this normalization, the $\log_2$ fold change of the normalized fragment ion current intensity was calculated between $SF_5^{\bullet+}$ and $C_{16}H_{10}^{\bullet+}$. All precursor ion populations were reacted to the 2τ time point (i.e., 13.5 ± 3% unreacted precursor ion current remaining in the MS/MS spectrum)

sequence informative $a^{\bullet}$- and *x-type* fragment ions produced when all accessible charge states of the three standard peptides were reacted with $SF_5^{\bullet+}$ or $C_{16}H_{10}^{\bullet+}$. Use of $SF_5^{\bullet+}$ as the reagent cation more than quadrupled the $a^{\bullet}$-*type* ion signal relative to $C_{16}H_{10}^{\bullet+}$ for all doubly deprotonated precursors. An increase in *x-type* fragment ion production was observed for two out of three doubly deprotonated precursors.

As charge density increased, the difference in fragment ion production was reduced. In the case of triply deprotonated precursors, $SF_5^{\bullet+}$ generated spectra with more $a^{\bullet}$-*type* fragment ions, whereas use of $C_{16}H_{10}^{\bullet+}$ cations produced more *x-type* fragment ions, but the magnitude of the difference is considerably less than for the lower charge state precursors. Generally, the $C_{16}H_{10}^{\bullet+}$ reagent cation produced spectra with marginally more *x-type* fragment ions for higher charge state species, but the product ion signal is largely comparable between the two reagent cations for $z \geq 3$ precursors. This suggests that the higher IE of $SF_5^{\bullet+}$ can benefit fragmentation of low charge density precursors (i.e., $z = -2$) where the predominance of NETnoD can adversely affect dissociation product ion generation. Note, however, $SF_5^{\bullet+}$ reagent cations retain the good performance of $C_{16}H_{10}^{\bullet+}$ for more highly charged ions. Supplementary Figure 3 also considers the distribution of even and odd electron fragment ions (odd electron species containing a radical electron and an additional hydrogen atom), showing that $a^{\bullet}$-*type* and *x-type* fragment ions are the predominant

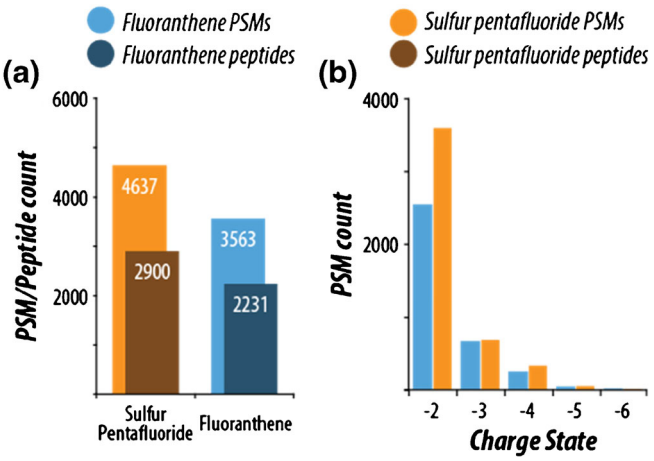

Figure 2. Summary of peptide spectral matches (PSM) and unique peptide identifications from nLC-MS/MS experiments using a yeast tryptic digest (**a**). Experiments were conducted using either $SF_5^{\bullet+}$ or $C_{16}H_{10}^{\bullet+}$ as reagent cations. The charge state distributions of successfully sequenced PSMs from these experiments are also shown (**b**), revealing a significant increase in $z = -2$ peptides identified with $SF_5^{\bullet+}$

species formed upon NETD, and that there is no significant difference in the even and odd electron ratios between the two reagent cations.

nLC-MS/MS of Yeast Tryptic Digest Using $SF_5^{\bullet+}$ and $C_{16}H_{10}^{\bullet+}$

To expand the scope of our study, we compared the performance of $C_{16}H_{10}^{\bullet+}$ and $SF_5^{\bullet+}$ as reagent cations in nLC-MS/MS analyses of peptides derived following tryptic digestion of yeast proteins. Importantly, the majority of precursors sampled in negative mode nLC-MS/MS experiments are doubly deprotonated [16], suggesting that the use of $SF_5^{\bullet+}$ reagent cations could improve the depth of analysis in whole-proteome shotgun sequencing. Indeed, in 90-min nLC-MS/MS experiments, NETD with $SF_5^{\bullet+}$ generated 30% more PSM and unique peptide identifications than did NETD using $C_{16}H_{10}^{\bullet+}$ (Figure 2). Figure 2b displays the charge state distribution of peptide spectral matches (PSMs) following use of the two NETD reagents. We note a substantial increase in the identification of $z = -2$ peptides for analyses with $SF_5^{\bullet+}$ (1039 more $z = -2$ PSMs than those with $C_{16}H_{10}^{\bullet+}$), which comprised more than 70% of all PSMs identified in either dataset. This finding is consistent with the previous results using standard peptides, further showing that peptides with lower charge density benefit more from excess recombination energy, while higher charge density peptides are not as impacted.

Figure 3 presents representative spectra from the nLC-MS/MS experiments illustrating the improved fragmentation afforded by use of $SF_5^{\bullet+}$ reagent cations as compared to $C_{16}H_{10}^{\bullet+}$. For each spectrum, the doubly deprotonated precursor of the peptide ETAESYLGAK was reacted with either NETD reagent to a reaction extent of 37.9% and 38.4% for $C_{16}H_{10}^{\bullet+}$ and $SF_5^{\bullet+}$, respectively. Reaction extent is defined as the ion current of the unreacted precursor divided by the total ion current of the scan. While in the standard peptide infusion data, a 0 nce CAD scan was used to measure the total ion abundance for each peptide and fragment ion currents could be normalized to it, allowing direct calculation of the precursor to product ion conversion ratio, in the discovery nLC-MS experiments no 0 nce CAD scans were performed and, therefore, this normalization approach was not possible, and reaction extent was calculated instead. Comparing spectra with similar reaction extents ensures that the main contributor to the difference is the ion chemistries of the reagents themselves. The spectra show many similarities but with considerably more product ions generated when $SF_5^{\bullet+}$ was used. Specifically, $SF_5^{\bullet+}$ produced two more $a^{\bullet}$-*type* and three more *x-type* fragment ions than the corresponding NETD spectrum produced when $C_{16}H_{10}^{\bullet+}$ was used as the reagent, and it also generated three CO_2 neutral losses from *x-type* fragment ions compared with

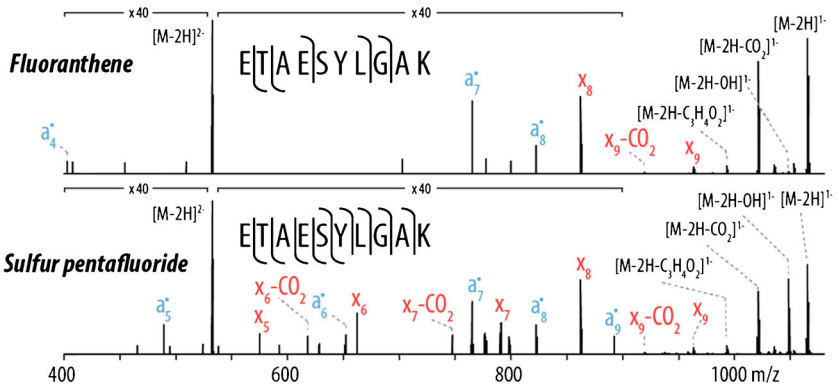

Figure 3. Single-scan spectra for the NETD fragmentation of the peptide ETAESYLGAK, $z = -2$. The unreacted precursor signal accounts for 37.9% and 38.4% of the total ion current in each MS/MS scan for $C_{16}H_{10}^{\bullet+}$ and $SF_5^{\bullet+}$, respectively, indicating both precursors were reacted to similar extents. Use of $SF_5^{\bullet+}$ as the NETD reagent provided greater sequence coverage than $C_{16}H_{10}^{\bullet+}$, yielding 11 sequence informative fragment ions compared with 5 for $C_{16}H_{10}^{\bullet+}$. The NETD reagent $SF_5^{\bullet+}$ produced three CO_2 product ion neutral loss species while the fluoranthene spectrum only contains a single CO_2 product ion neutral loss fragment. Both spectra were acquired in the nLC-MS/MS experiments and represent a single scan (i.e., un-averaged)

only one when $C_{16}H_{10}^{\bullet+}$ cations were used. In all, use of $SF_5^{\bullet+}$ as the reagent cation produced a spectrum with 100% peptide sequence coverage for ETAESYLGAK, whereas the corresponding spectrum when $C_{16}H_{10}^{\bullet+}$ was used as the reagent yields only 55.5% coverage. Note, we define peptide sequence coverage as the ratio of the number of inter-residue positions broken to the total possible positions (residue length – 1) for a given sequence, expressed here as a percentage.

Figure 4a expands on the change in peptide sequence coverage between reagent cations $SF_5^{\bullet+}$ and $C_{16}H_{10}^{\bullet+}$ by showing the composite difference for all peptides identified in the NETD experiments. Only peptides found in both data sets were considered, and of the 1427 peptides in common, 812 peptides yielded an increase in sequence coverage when $SF_5^{\bullet+}$ was used as the NETD reagent while only a fourth of that (n = 202) showed an increase when $C_{16}H_{10}^{\bullet+}$ was used. On average, $SF_5^{\bullet+}$ accounted for a nearly 10% improvement in peptide sequence coverage for all overlapping peptides.

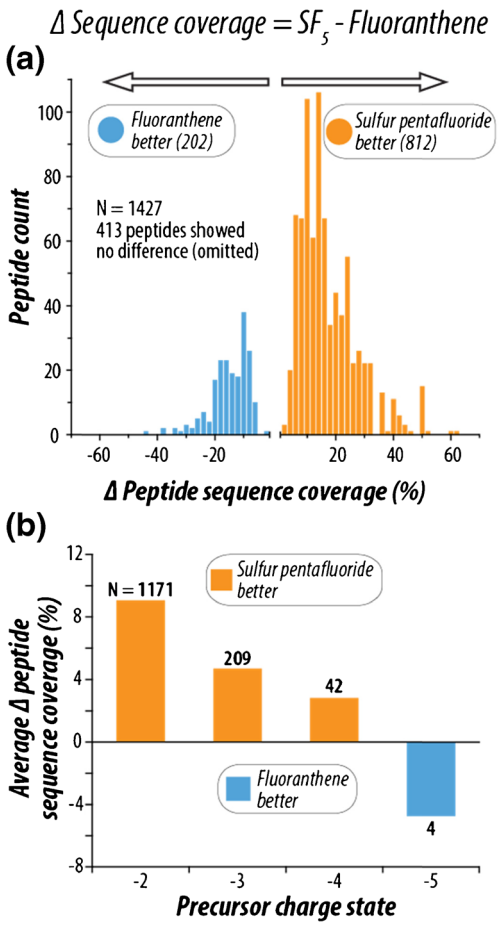

Figure 4. (**a**) Percent peptide sequence coverage was calculated for each of the 1427 peptides in common between the $SF_5^{\bullet+}$ and $C_{16}H_{10}^{\bullet+}$ analyses. The difference between peptide sequence coverage with $SF_5^{\bullet+}$ and $C_{16}H_{10}^{\bullet+}$ (*Δ Peptide Sequence Coverage*) was calculated for each peptide, and the distribution of the *Δ Peptide Sequence Coverage* values are shown. The orange distribution shows peptides with greater sequence coverage with $SF_5^{\bullet+}$ (n = 812), and the blue shows peptides with better sequence coverage with $C_{16}H_{10}^{\bullet+}$ (n = 202). Panel (**b**) shows the average *Δ Peptide Sequence Coverage* for all peptides in common between the two analyses as a function of peptide precursor charge state. The number of precursors averaged is shown in black text above the bar for each charge state. Concordant with previously shown data, lower charged precursors benefit most from the use of $SF_5^{\bullet+}$

Differences in peptide sequence coverage are even more pronounced when delineating across charge states. Figure 4b displays peptides categorized by charge state, where charge states of $z = -2$, –3, –4, and –5 showed an average sequence coverage difference of 9.0%, 4.7%, 2.8%, and –4.7%, respectively. Note, as indicated in the ΔSequence Coverage equation at the top of Figure 4, a positive value indicates higher sequence coverage with $SF_5^{\bullet+}$. Interestingly, $C_{16}H_{10}^{\bullet+}$ as the NETD reagent only performs better on $z = -5$ precursors, which account for 1.3% of the total precursors sampled in the experiments. In all other cases, peptide sequence coverage was improved by use of $SF_5^{\bullet+}$, especially for lower precursor charge states. Supplementary Figure 4 considers the impact of reagent cation on total protein sequence coverage for all proteins in common between the two data sets, as the increased number of peptide identifications with $SF_5^{\bullet+}$ translates to high coverage of the proteins mapped in the experiments. Here, protein sequence coverage is defined as the number of amino acid residues comprising each identified peptide divided by all amino acid residues in the protein sequence. Use of $SF_5^{\bullet+}$ improved coverage of 298 proteins, $C_{16}H_{10}^{\bullet+}$ improved coverage of 125 proteins, and 84 showed no difference between the reagent cations, with an average improvement of 3.1% in favor of $SF_5^{\bullet+}$.

Comparison of Neutral Losses

Utilizing the higher ionization energy $SF_5^{\bullet+}$ reagent cation yields greater fragmentation in regards to sequence informative fragment ions. As the Polfer group noted with xenon, however, high ionization energies can drive the production of neutral losses from fragment ions. Using the same pool of doubly deprotonated peptides in common between the $C_{16}H_{10}^{\bullet+}$ and $SF_5^{\bullet+}$ data sets discussed above, Figure 5 examines how the oxidized (i.e., charge-reduced) precursor ions and their associated neutral losses are affected by the use of the two reagent cations. Figure 5a displays the average percent ion current accounted for by the oxidized precursor as well as the signal from corresponding neutral losses of CO_2 and either NH_3 or OH from this charge-reduced species. Doubly charged peptide precursors reacted with $C_{16}H_{10}^{\bullet+}$ show on average 8.5% more CO_2 neutral loss while the $SF_5^{\bullet+}$ data yielded greater NH_3 and OH neutral loss. Figure 5b compares the abundance of amino acid-specific side chain neutral losses from the oxidized precursor [12]. The predominant differences are found in methionine, serine, and threonine residues. Interestingly, methionine and serine show a substantial increase in neutral loss when $C_{16}H_{10}^{\bullet+}$ is used, despite the lower recombination energy relative to $SF_5^{\bullet+}$. However, in total, very little difference is found in amino acid-specific side chain neutral loss when comparing the two NETD reagent cations.

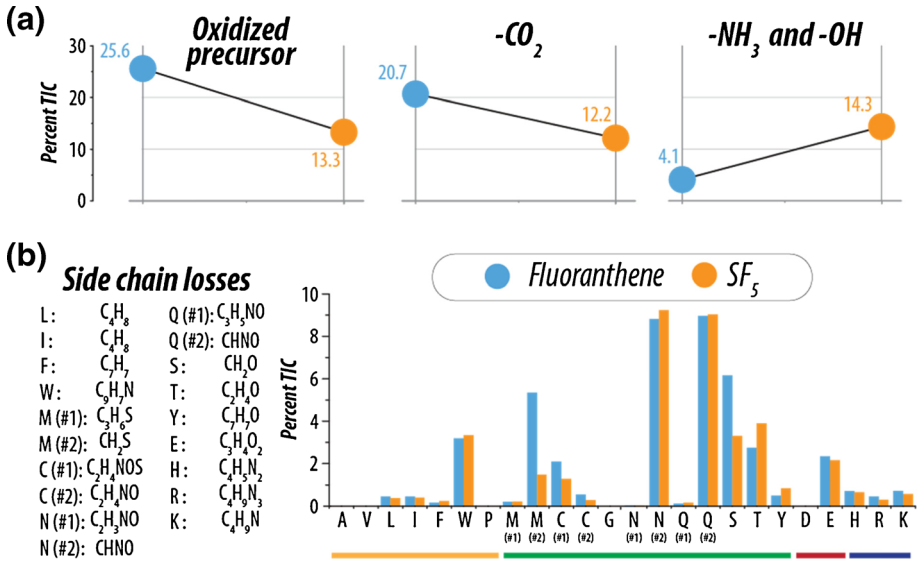

Figure 5. (**a**) The average percent of total ion current accounted for by the oxidized precursor ion and neutral losses of CO_2 and either NH_3 or OH from the oxidized precursor ion are shown for $z = -2$ PSMs from $C_{16}H_{10}^{\bullet+}$ (blue) and $SF_5^{\bullet+}$ (orange) nLC-MS/MS analyses. (**b**) The average percent of total ion current is shown for side chain neutral losses from the oxidized precursor ion for $z = -2$ PSMs. In order for a spectrum to be searched for a given side chain loss, the PSM sequence had to contain that residue. Note, amino acids are organized by their side chain properties: nonpolar (yellow), polar (green), acidic (red), and basic (blue)

Lastly, we investigated the $a^{\bullet}$- and *x-type* product ions generated in these experiments, including how CO_2 neutral losses from product ions differed between the two reagent cations. Figure 6a provides a holistic look at the total number of $a^{\bullet}$- and *x-type* fragment ions produced in the NETD datasets. As shown with our standard peptide data above, $SF_5^{\bullet+}$ yields more fragment ions species than $C_{16}H_{10}^{\bullet+}$, particularly more $a^{\bullet}$-*type* fragments, with an increase of 32%. Figure 6b shows the percentage of those sequence ions that also yield a CO_2 neutral loss peak. $SF_5^{\bullet+}$ cations generated 5.4% more *x-type* ion species with CO_2 neutral losses. To investigate how the occurrence of these neutral losses from sequencing ions impacts data analysis, we searched our yeast peptide database allowing for a variety of different fragment ion combinations. No combination of product ions and neutral losses yielded a greater number of PSMs when searching the $SF_5^{\bullet+}$ dataset than just $a^{\bullet}$- and *x-type* fragment ions alone, which concurs with the same analysis performed on the fluoranthene dataset (not shown). We conclude that the amount of CO_2 neutral loss is not significant enough to impact or adversely affect automated spectral annotation.

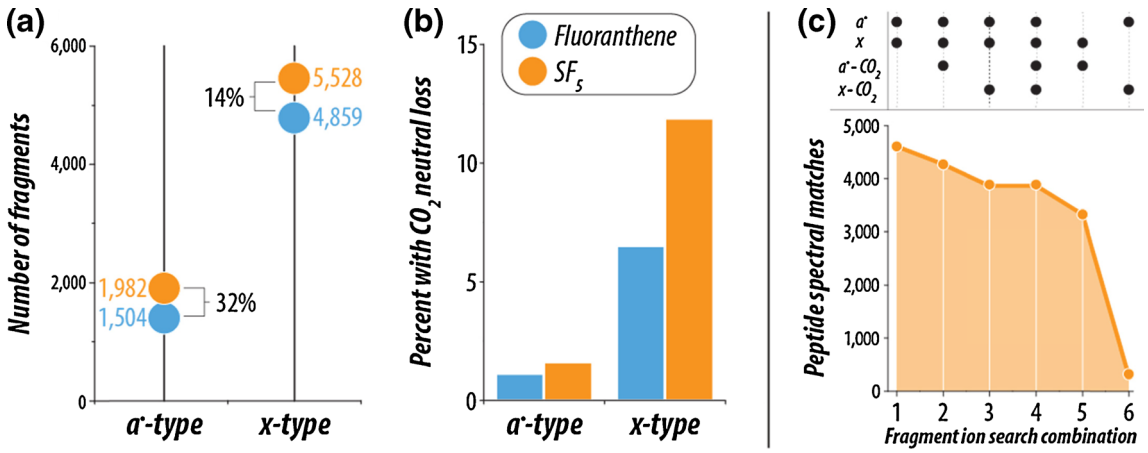

Figure 6. (**a**) The number of total $a^{\bullet}$- and *x-type* fragment ions generated from the peptides common to both $C_{16}H_{10}^{\bullet+}$ (blue) and $SF_5^{\bullet+}$ (orange) analyses are shown. For both fragment ion types $SF_5^{\bullet+}$ produces the greater number of sequencing ions, and the percent gains over the number of ions from $C_{16}H_{10}^{\bullet+}$ analyses are shown in bold. Panel (**b**) compares the percentage of $a^{\bullet}$- and *x-type* product ions from Panel (**a**) that have a corresponding neutral loss of CO_2. (**c**) Despite the small increase in CO_2 neutral losses observed, incorporating CO_2 neutral losses from $a^{\bullet}$- and *x-type* product ions as fragment ion types to query in a database search does not improve peptide identifications over using standard $a^{\bullet}$- and *x-type* product ions only for the $SF_5^{\bullet+}$ data. The combination of product ion types used in the database searches are shown in black at the top, and the number of identified peptide spectral matches are shown in orange at the bottom. Similar results were obtained with the $C_{16}H_{10}^{\bullet+}$ analyses (data not shown)

Conclusion

NETD provides direct access to analysis of proteomes in the negative mode, but improvements are still needed to make NETD amenable to the large proportion of low charge density precursors generated in whole-proteome analyses. In this experiment, we sought to improve peptide anion fragmentation using $SF_5^{\bullet+}$, a reagent cation with a higher IE of 9.6 eV, compared with $C_{16}H_{10}^{\bullet+}$, the most common NETD reagent cation with an IE of 7.9 eV. Using peptide fragmentation efficiency and unique peptide identifications as our primary metrics, we determined that $SF_5^{\bullet+}$ significantly improves shotgun proteomic analyses with NETD, especially considering the fragmentation of doubly deprotonated precursors. We contribute this gain in identification power to the increase in ionization energy for $SF_5^{\bullet+}$ compared with $C_{16}H_{10}^{\bullet+}$, which impacts the exothermicity of the ion–ion reaction and provides greater fragment ion yield and less non-dissociative negative electron transfer. The predominant gain in identification for low charge density precursors may also be useful when considering protein digestion using proteases other than trypsin, such as Lys-C, which often yields longer, less charge-dense peptides. Another benefit of using a gaseous reagent for NETD is the simplification of the ion source as no reagent vial heaters or heated transfer lines are required to volatilize and transfer the solid fluoranthene reagent.

Although $SF_5^{\bullet+}$ appears to be a favorable choice for large-scale negative mode proteomics analyses, its use in other types of NETD applications may benefit as well. While previous work has shown that lower recombination energy NETD reactions reduce the occurrence of labile PTM neutral loss [43], many other molecules might benefit from the more energetic reaction. In addition to peptides, NETD has been useful in the study of polynucleotides [35] and carbohydrates [50–53], and further improvements may be obtained through the utilization of $SF_5^{\bullet+}$ as the reagent cation.

Acknowledgements

The authors gratefully acknowledge support from Thermo Fisher Scientific and NIH grant R35 GM118110. N.M.R. was funded through an NIH Predoctoral to Postdoctoral Transition Award (F99 CA212454).

References

1. Kim, M.S., Pinto, S.M., Getnet, D., Nirujogi, R.S., Manda, S.S., Chaerkady, R., Madugundu, A.K., Kelkar, D.S., Isserlin, R., Jain, S., Thomas, J.K., Muthusamy, B., Leal-Rojas, P., Kumar, P., Sahasrabuddhe, N.A., Balakrishnan, L., Advani, J., George, B., Renuse, S., Selvan, L.D.N., Patil, A.H., Nanjappa, V., Radhakrishnan, A., Prasad, S., Subbannayya, T., Raju, R., Kumar, M., Sreenivasamurthy, S.K., Marimuthu, A., Sathe, G.J., Chavan, S., Datta, K.K., Subbannayya, Y., Sahu, A., Yelamanchi, S.D., Jayaram, S., Rajagopalan, P., Sharma, J., Murthy, K.R., Syed, N., Goel, R., Khan, A.A., Ahmad, S., Dey, G., Mudgal, K., Chatterjee, A., Huang, T.-C., Zhong, J., Wu, X., Shaw, P.G., Freed, D., Zahari, M.S., Mukherjee, K.K., Shankar, S., Mahadevan, A., Lam, H., Mitchell, C.J., Shankar, S.K., Satishchandra, P., Schroeder, J.T., Sirdeshmukh, R., Maitra, A., Leach, S.D., Drake, C.G., Halushka, M.K., Prasad, T.S.K., Hruban, R.H., Kerr, C.L., Bader, G.D., Iacobuzio-Donahue, C.A., Gowda, H., Pandey, A.: A draft map of the human proteome. Nature **509**, 575–581 (2014)
2. Wilhelm, M., Schlegl, J., Hahne, H., Moghaddas Gholami, A., Lieberenz, M., Savitski, M.M., Ziegler, E., Butzmann, L., Gessulat, S., Marx, H., Mathieson, T., Lemeer, S., Schnatbaum, K., Reimer, U., Wenschuh, H., Mollenhauer, M., Slotta-Huspenina, J., Boese, J.-H., Bantscheff, M., Gerstmair, A., Faerber, F., Kuster, B.: Mass-spectrometry-based draft of the human proteome. Nature **509**, 582–587 (2014)
3. Hebert, A.S., Richards, A.L., Bailey, D.J., Ulbrich, A., Coughlin, E.E., Westphall, M.S., Coon, J.J.: The 1 hour yeast proteome. Mol. Cell. Proteomics **13**, 339–347 (2014)
4. Richards, A.L., Merrill, A.E., Coon, J.J.: Proteome sequencing goes deep. Curr. Opin. Chem. Biol. **24C**, 11–17 (2015)
5. Riley, N.M., Hebert, A.S., Coon, J.J.: Proteomics moves into the fast lane. Cell Syst. **2**, 142–143 (2016)
6. Yamashita, M., Fenn, J.B.: Negative ion production with the electrospray ion source. J. Phys. Chem. **88**, 4671–4675 (1984)
7. Fenn, J.B., Mann, M., Meng, C.K., Wong, S.F., Whitehouse, C.M.: Electrospray ionization for mass spectrometry of large biomolecules. Science **246**, 64–71 (1989)
8. Straub, R.F., Voyksner, R.D., Voyksner, D.: Negative ion formation in electrospray mass spectrometry. J. Am. Soc. Mass Spectrom. **4**, 578–587 (1993)
9. Brinkworth, C.S., Dua, S., McAnoy, A.M., Bowie, J.H.: Negative ion fragmentations of deprotonated peptides: backbone cleavages directed through both Asp and Glu. Rapid Commun. Mass Spectrom. **15**, 1965–1973 (2001)
10. Bowie, J.H., Brinkworth, C.S., Dua, S.: Collision-induced fragmentations of the (M – H)-parent anions of underivatized peptides: an aid to structure determination and some unusual negative ion cleavages. Mass Spectrom. Rev. **21**, 87–107 (2002)
11. Coon, J.J., Shabanowitz, J., Hunt, D.F., Syka, J.E.P.: Electron transfer dissociation of peptide anions. J. Am. Soc. Mass Spectrom. **16**, 880–882 (2005)
12. Rumachik, N.G., McAlister, G.C., Russell, J.D., Bailey, D.J., Wenger, C.D., Coon, J.J.: Characterizing peptide neutral losses induced by negative electron-transfer dissociation (NETD). J. Am. Soc. Mass Spectrom. **23**, 718–727 (2012)
13. Flora, J.W., Muddiman, D.C.: Selective, sensitive, and rapid phosphopeptide identification in enzymatic digests using ESI-FTICR-MS with infrared multiphoton dissociation. Anal. Chem. **73**, 3305–3311 (2001)
14. Madsen, J.A., Kaoud, T.S., Dalby, K.N., Brodbelt, J.S.J.S.: 193-nm Photodissociation of singly and multiply charged peptide anions for acidic proteome characterization. Proteomics **11**, 1329–1334 (2011)
15. Shaw, J.B., Kaplan, D.A., Brodbelt, J.S.: Activated ion negative electron transfer dissociation of multiply charged peptide anions. Anal. Chem. **85**, 4721–4728 (2013)
16. Riley, N.M., Rush, M.J.P., Rose, C.M., Richards, A.L., Kwiecien, N.W., Bailey, D.J., Hebert, A.S., Westphall, M.S., Coon, J.J.: The negative mode proteome with activated ion negative electron transfer dissociation. Mol. Cell. Proteomics **14**, 2644–2660 (2015)
17. McAlister, G.C., Russell, J.D., Rumachik, N.G., Hebert, A.S., Syka, J.E.P., Geer, L.Y., Westphall, M.S., Pagliarini, D.J., Coon, J.J.: Analysis of the acidic proteome with negative electron-transfer dissociation mass spectrometry. Anal. Chem. **84**, 2875–2882 (2012)
18. Cook, S.L., Jackson, G.P.: Metastable atom-activated dissociation mass spectrometry of phosphorylated and sulfonated peptides in negative ion mode. J. Am. Soc. Mass Spectrom. **22**, 1088–1099 (2011)
19. Smith, S.A., Kalcic, C.L., Cui, L., Reid, G.E.: Femtosecond laser-induced ionization/dissociation tandem mass spectrometry (fsLID-MS/MS) of deprotonated phosphopeptide anions. Rapid Commun. Mass Spectrom. **27**, 2807–2817 (2013)
20. Jai-nhuknan, J., Cassady, C.J.: Negative ion postsource decay time-of-flight mass spectrometry of peptides containing acidic amino acid residues. Anal. Chem. **70**, 5122–5128 (1998)
21. Larraillet, V., Antoine, R., Dugourd, P., Lemoine, J.: Activated-electron photodetachment dissociation for the structural characterization of protein polyanions. Anal. Chem. **81**, 8410–8416 (2009)
22. Larraillet, V., Vorobyev, A., Brunet, C., Lemoine, J., Tsybin, Y.O., Antoine, R., Dugourd, P.: Comparative dissociation of peptide polyanions by electron impact and photo-induced electron detachment. J. Am. Soc. Mass Spectrom. **21**, 670–680 (2010)

23. Antoine, R., Joly, L., Tabarin, T., Broyer, M., Dugourd, P., Lemoine, J.: Photo-induced formation of radical anion peptides. Electron photodetachment dissociation experiments. Rapid Commun. Mass Spectrom. **21**, 265–268 (2007)
24. Haselmann, K., Budnik, B., Kjeldsen, F., Nielsen, M., Olsen, J., Zubarev, R.: Electronic excitation gives informative fragmentation of polypeptide cations and anions. Eur. J. Mass Spectrom. **8**, 117 (2002)
25. Kjeldsen, F., Silivra, O.A., Ivonin, I.A., Haselmann, K.F., Gorshkov, M., Zubarev, R.A.: Cα–C backbone fragmentation dominates in electron detachment dissociation of gas-phase polypeptide polyanions. Chem. Eur. J. **11**, 1803–1812 (2005)
26. Halim, M.A., Girod, M., MacAleese, L., Lemoine, J., Antoine, R., Dugourd, P.: 213 nm Ultraviolet photodissociation on peptide anions: radical-directed fragmentation patterns. J. Am. Soc. Mass Spectrom. **27**, 474–486 (2016)
27. Greer, S.M., Cannon, J.R., Brodbelt, J.S.: Improvement of shotgun proteomics in the negative mode by carbamylation of peptides and ultraviolet photodissociation mass spectrometry. Anal. Chem. **86**, 12285–12290 (2014)
28. Robinson, M.R., Moore, K.L., Brodbelt, J.S.: Direct identification of tyrosine sulfation by using ultraviolet photodissociation mass spectrometry. J. Am. Soc. Mass Spectrom. **25**, 1461–1471 (2014)
29. Madsen, J.A., Xu, H., Robinson, M.R., Horton, A.P., Shaw, J.B., Giles, D.K., Kaoud, T.S., Dalby, K.N., Trent, M.S., Brodbelt, J.S.: High-throughput database search and large-scale negative polarity liquid chromatography-tandem mass spectrometry with ultraviolet photodissociation for complex proteomic samples. Mol. Cell. Proteomics **12**, 2604–2614 (2013)
30. Riley, N.M., Bern, M., Westphall, M.S., Coon, J.J.: A full-featured search algorithm for negative electron transfer dissociation. J. Proteome Res. **15**, 2768–2776 (2016)
31. Prentice, B.M., McLuckey, S.A.: Gas-phase ion/ion reactions of peptides and proteins: acid/base, redox, and covalent chemistries. Chem. Commun. (Camb.) **49**, 947–965 (2013)
32. McLuckey, S.A., Mentinova, M.: Ion/neutral, ion/electron, ion/photon, and ion/ion interactions in tandem mass spectrometry: do we need them all? Are they enough? J. Am. Soc. Mass Spectrom. **22**, 3–12 (2011)
33. Herron, W.J., Goeringer, D.E., McLuckey, S.A.: Gas-phase electron-transfer reactions from multiply-charged anions to rare-gas cations. J. Am. Chem. Soc. **117**, 11555–11562 (1995)
34. Gao, Y., Yang, J., Cancilla, M.: Top-down interrogation of chemically modified oligonucleotides by negative electron transfer and collision induced dissociation. Anal. Chem. (2013)
35. Huang, T.Y., McLuckey, S.A.: Gas-phase ion/ion reactions of rubrene cations and multiply charged DNA and RNA anions. Int. J. Mass Spectrom. **304**, 140–147 (2011)
36. Horn, D.M., Ge, Y., McLafferty, F.W.: Activated ion electron capture dissociation for mass spectral sequencing of larger (42 kDa) proteins. Anal. Chem. **72**, 4778–4784 (2000)
37. Xia, Y., Gunawardena, H.P., Erickson, D.E., McLuckey, S.A.: Effects of cation charge-site identity and position on electron-transfer dissociation of polypeptide cations. J. Am. Chem. Soc. **129**, 12232–12243 (2007)
38. Shaw, J.B., Madsen, J.A., Xu, H., Brodbelt, J.S.: Systematic comparison of ultraviolet photodissociation and electron transfer dissociation for peptide anion characterization. J. Am. Soc. Mass Spectrom. **23**, 1707–1715 (2012)
39. Swaney, D.L., McAlister, G.C., Wirtala, M., Schwartz, J.C., Syka, J.E., Coon, J.J.: Supplemental activation method for high-efficiency electron-transfer dissociation of doubly protonated peptide precursors. Anal. Chem. **79**, 477–485 (2007)
40. Hamidane, H.B., Chiappe, D., Hartmer, R., Vorobyev, A., Moniatte, M., Tsybin, Y.O.: Electron capture and transfer dissociation: peptide structure analysis at different ion internal energy levels. J. Am. Soc. Mass Spectrom. **20**, 567–575 (2009)
41. Ledvina, A.R., Rose, C.M., McAlister, G.C., Syka, J.E.P., Westphall, M.S., Griep-Raming, J., Schwartz, J.C., Coon, J.J.: Activated ion ETD performed in a modified collision cell on a hybrid QLT-Oribtrap mass spectrometer. J. Am. Soc. Mass Spectrom. **24**, 1623–1633 (2013)
42. Gunawardena, H.P., He, M., Chrisman, P.A., Pitteri, S.J., Hogan, J.M., Hodges, B.D.M., McLuckey, S.A.: Electron transfer versus proton transfer in gas-phase ion/ion reactions of polyprotonated peptides. J. Am. Chem. Soc. **127**, 12627–12639 (2005)
43. Huzarska, M., Ugalde, I., Kaplan, D.A., Hartmer, R., Easterling, M.L., Polfer, N.C.: Negative electron transfer dissociation of deprotonated phosphopeptide anions: choice of radical cation reagent and competition between electron and proton transfer. Anal. Chem. **82**, 2873–2878 (2010)
44. Crizer, D.M., Xia, Y., McLuckey, S.A.: Transition metal complex cations as reagents for gas-phase transformation of multiply deprotonated polypeptides. J. Am. Soc. Mass Spectrom. **20**, 1718–1722 (2009)
45. Ledvina, A.R., Beauchene, N.A., McAlister, G.C., Syka, J.E., Schwartz, J.C., Griep-Raming, J., Westphall, M.S., Coon, J.J.: Activated-ion electron transfer dissociation improves the ability of electron transfer dissociation to identify peptides in a complex mixture. Anal. Chem. **82**, 10068–10074 (2010)
46. Rose, C.M., Russell, J.D., Ledvina, A.R., McAlister, G.C., Westphall, M.S., Griep-Raming, J., Schwartz, J.C., Coon, J.J., Syka, J.E.P.: Multipurpose dissociation cell for enhanced ETD of intact protein species. J. Am. Soc. Mass Spectrom. **24**, 816–827 (2013)
47. Riley, N.M., Westphall, M.S., Coon, J.J.: Activated ion electron transfer dissociation for improved fragmentation of intact proteins. Anal. Chem. **87**, 7109–7116 (2015)
48. Geer, L.Y., Markey, S.P., Kowalak, J.A., Wagner, L., Xu, M., Maynard, D.M., Yang, X., Shi, W., Bryant, S.H.: Open mass spectrometry search algorithm. J. Proteome Res. **3**, 958–964 (2004)
49. Rose, C.M., Rush, M.J.P., Riley, N.M., Merrill, A.E., Kwiecien, N.W., Holden, D.D., Mullen, C., Westphall, M.S., Coon, J.J.: A calibration routine for efficient ETD in large-scale proteomics. J. Am. Soc. Mass Spectrom. **26**, 1848–1857 (2015)
50. Wolff, J.J., Leach III, F.E., Laremore, T.N., Kaplan, D.A., Easterling, M.L., Linhardt, R.J., Amster, I.J.: Negative electron transfer dissociation of glycosaminoglycans. Anal. Chem. **82**, 3460–3466 (2010)
51. Leach III, F.E., Wolff, J.J., Xiao, Z., Ly, M., Laremore, T.N., Arungundram, S., Al-Mafraji, K., Venot, A., Boons, G.J., Linhardt, R.J., Amster, I.J.: Negative electron transfer dissociation Fourier transform mass spectrometry of glycosaminoglycan carbohydrates. Eur. J. Mass Spectrom. (Chichester, Engl.) **17**, 167–176 (2011)
52. Huang, Y., Yu, X., Mao, Y., Costello, C.E., Zaia, J., Lin, C.: De novo sequencing of heparan sulfate oligosaccharides by electron-activated dissociation. Anal. Chem. **85**, 11979–11986 (2013)
53. Hu, H., Huang, Y., Yu, X., Yongmei, X., Liu, J., Zong, C., Boons, G.-J., Lin, C., Xia, Y., Zaia, J.: A computational framework for heparan sulfate sequencing using high-resolution tandem mass spectra. Mol. Cell. Proteomics **13**, 2490–2502 (2014)